Nuclear Instruments and Methods in Physics Research B 343 (2015) 123–131

Contents lists available at ScienceDirect

Nuclear Instruments and Methods in Physics Research B

journal homepage: www.elsevier.com/locate/nimb

# A novel double hohlraum target to create a moderately coupled plasma for ion stopping experiments

A. Ortner [a,e,*], S. Faik [c], D. Schumacher [b], M.M. Basko [d,e,b], A. Blazevic [b,f], S. Busold [a,b,f], S. Bedacht [a], W. Cayzac [b], A. Frank [f], D. Kraus [g], T. Rienecker [c], G. Schaumann [a], An. Tauschwitz [e,c], F. Wagner [a], M. Roth [a]

[a] Institut für Kernphysik, Technische Universität Darmstadt, Schlossgartenstrasse 9, 64289 Darmstadt, Germany
[b] GSI Helmholtzzentrum für Schwerionenforschung GmbH, Planckstr. 1, 64291 Darmstadt, Germany
[c] Goethe-Universität Frankfurt am Main, Max-von-Laue-Str. 1, 60438 Frankfurt am Main, Germany
[d] Keldysh Institute of Applied Mathematics (KIAM), Miusskaya sq. 4, 125047 Moscow, Russia
[e] Helmholtz International Center for FAIR (HIC for FAIR), Max-von-Laue-Str. 1, 60438 Frankfurt am Main, Germany
[f] Helmholtz-Institut Jena, Fröbelstieg 3, 07743 Jena, Germany
[g] University of California, Berkeley, USA

ARTICLE INFO

*Article history:*
Received 14 September 2014
Received in revised form 12 November 2014
Accepted 14 November 2014

*Keywords:*
Ion stopping in plasma
Coupled plasma
Non-ideal plasma
2D hydrodynamics
Hohlraum radiation

ABSTRACT

We present a new double hohlraum target for the creation of a moderately coupled ($0.1 < \Gamma < 1$) carbon plasma for energy loss and charge state measurements of projectile ions interacting with this plasma. A spherical cavity of 600 μm in diameter is heated with a 150-J laser pulse ($\lambda_L = 527$ nm) within 1.2 ns to produce a quasi-Planckian X-ray source with a radiation temperature of $T_r \approx 100$ eV. These X-rays are then used to heat volumetrically two thin carbon foils in a secondary cylindrical hohlraum to a dense plasma state. An axi-symmetric plasma column with a free-electron density of up to $8 \times 10^{21}$ cm$^{-3}$, a temperature of $T \approx 10$ eV, and an average ionization degree of $Z \approx 3$ is generated. This plasma stays in a dense and an almost uniform state for about 5 ns. Ultimately, such targets are supposed to be used in experiments where a heavy ion beam is launched through the sample plasma, and the ion energy losses as well as the charge distributions are to be measured. The present paper is in a certain sense a symbiotic one, where the theoretical analysis and the experimental results are combined to investigate the basic properties and the prospects of this type of plasma targets.



## 1. Introduction

The knowledge of the energy deposition by fast ions in a plasma is a key issue for the inertial confinement fusion (ICF) research, particularly for simulations of the α-particle heating, for the assessment of heavy ions as a potential driver (HIF) [1,2], and for the fast ignition (FI) [3] concept with ion beams. The stopping of heavy projectiles, traveling through ionized matter, depends strongly on its temperature, density and on its ionization degree.

Most experiments carried out in the past investigated the interaction of ions with an ideal, fully ionized plasma. First attempts in the 1990s used gas and Z-pinch discharges [4–7] to create fully ionized hydrogen plasmas. However, being generated from the gas phase, these plasmas have limited free electron densities $n_e \leq 10^{19}$ cm$^{-3}$ and relatively low temperatures of 2–3 eV. Much hotter, denser and almost fully ionized plasmas were achieved by direct irradiation of solid targets (like thin planar foils) with intense laser pulses [8,9]. These laser plasmas are typically spatially and temporally inhomogeneous because of a strongly non-uniform intensity distribution across the focal spot, and because of strong density and temperature variation between the rapidly expanding dilute undercritical corona and the dense overcritical region. The homogeneity can be improved to a certain degree by applying laser beam smoothing techniques like the use of random phase plates (RPP) or induced spatial incoherence (ISI), and by using frequency doubled or tripled laser light [10–12]. Nevertheless, as the laser energy is mainly deposited in the plasma corona up to the critical density, these plasmas are of relatively high temperature, typically ranging from 100 eV to 250 eV and with densities of $n_e \leq 5 \times 10^{20}$ cm$^{-3}$. This corresponds to an ideal plasma with $\Gamma \ll 1$, where $\Gamma$ is the electron–electron coupling parameter[1] defined as

* Corresponding author at: Institut für Kernphysik, Technische Universität Darmstadt, Schlossgartenstrasse 9, 64289 Darmstadt, Germany.
*E-mail address:* a.ortner@gsi.de (A. Ortner).

[1] In this paper we use the notation $\Gamma = \Gamma_{ee}$.

http://dx.doi.org/10.1016/j.nimb.2014.11.047
0168-583X/

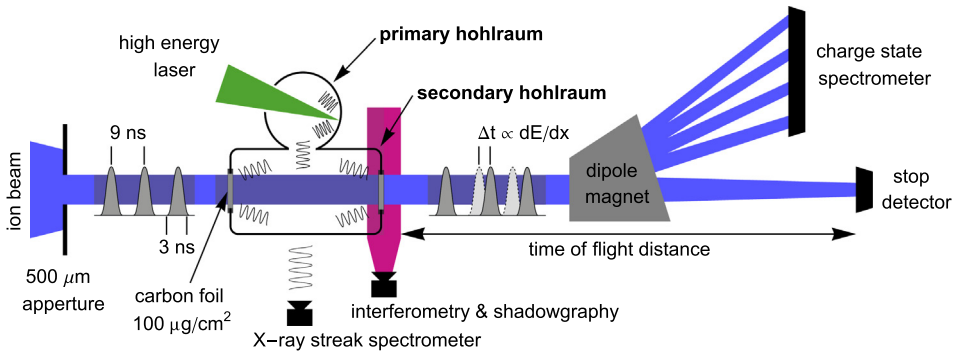


**Fig. 1.** Schematic of the experimental setup with the double hohlraum target, the ion beam and the diagnostics. The ion beam is trimmed to 500 μm by an aperture before entering the hohlraum; it is bunched in 3 ns long (FWHM) pulses coming every 9 ns. The delayed ion bunches are detected after a 12 m time of flight distance either in a stop detector or a charge state spectrometer. The hohlraum radiation is measured by an X-ray streak spectrometer, the free electron density and the plasma expansion by a multi-frame interferometry.

$$\Gamma = \frac{e^2}{k_B T_e}\left(\frac{4\pi}{3} n_e\right)^{1/3} \quad (1)$$

In the regime of partially ionized and moderately coupled[2] plasmas, hardly any experimental data for ion energy loss exists because of the difficulty to maintain such a plasma state for a sufficiently long time ($> 4$ ns). A few attempts have been made to compress and ionize the initial gas by a strong shock, generated by either an electromagnetic shock tube [13] or by an explosive-driven flyer plate [14]. The achieved electron densities of $n_e \approx 5 \times 10^{19}$ cm$^{-3}$ and plasma temperatures of 1–2 eV result in rather low ionization states and the values $0.4 < \Gamma < 1.5$ [15].

An appealing method to create a more uniform plasma state at intermediate temperatures and high densities is to apply volumetric heating of a solid sample with soft X-ray radiation [16,17]. For this method an intense laser pulse is used to generate a high-Z plasma, which serves as a strong source of X-rays [18]. If this source is placed inside a cavity made of high-Z material, the radiation gets confined because it indirectly heats the total inner wall of the cavity which then itself becomes a strong emitter of thermal soft X-ray radiation [19–22]. The absorbed and reemitted radiation establishes a spatially uniform temperature distribution in the cavity and serves as an intense, isotropic soft X-ray source with a quasi-thermal spectral distribution. By placing a sample material inside such a thermalized hohlraum the plasma is inertially and thermally confined, as hydrodynamic expansion is limited and the radiative cooling is suppressed.

However, because direct interaction of the laser radiation with the sample material has to be avoided, and since the target geometry needs to be adapted to be probed with an ion beam, such a hohlraum must consist of at least two chambers: one primary cavity for the absorption of the laser light and its conversion into an intense X-ray source, and a secondary chamber containing the sample material and shielding it against primary radiation (laser and hot-spot-radiation). For our double hohlraum we use a spherical cavity for the conversion of the laser light, and a cylindrical hohlraum aligned parallel to the ion beam axis to house a carbon foil sample.

First experimental investigations [23,24] of the properties of double hohlraums turned out to be insufficient for adequate understanding of these complex targets and theoretical simulations had to be added. In the following, the detailed experimental and theoretical results are presented. The investigated targets are supposed to be used in future experiments, which should for the first time allow to study interaction of fast ion beams with a non-ideal plasma. These investigations will be the next step to advance into the regime of non-linear ion stopping, where complex beam-plasma coupling effects are expected [25–27].

[2] Under "moderately coupled" we understand plasmas with coupling parameters in the range $0.1 < \Gamma \leq 1$.

## 2. Experimental methods

### 2.1. General concept

All the experiments (both accomplished and planned) discussed in this paper are carried out at the GSI Helmholtz center for heavy ion research in Darmstadt, Germany, where a unique possibility exists to combine a heavy ion beam with a high power laser. Here the ion beam, delivered by the UNILAC accelerator, and the high-energy nanosecond pulse option of the PHELIX laser [28] are used. The experimental setup is shown in Fig. 1. The laser beam is focused into a submillimeter spherical cavity, where it creates a hot plasma which serves as a primary X-ray source. This radiation heats up the secondary cylindrical hohlraum, where the sample material in the form of two thin carbon foils is placed. Both cavities are made of gold to achieve high conversion efficiency and an efficient radiation confinement. The two carbon foils, attached on either side of the secondary hohlraum, turn into a dense plasma column along the ion beam axis. This plasma is then probed by a bunched heavy ion beam. The ions interact with the plasma and lose a certain fraction of their energy. This energy loss is measured by detecting the delayed arrival of the ion bunch after a time-of-flight distance. In addition, the charge state distribution can be measured with a magnetic dipole spectrometer. Both measurements are carried out as time resolved. For this kind of measurements, it is of crucial importance that the interaction path of the ion beam stays free from gold ablated from the inner hohlraum walls for at least the duration of one ion bunch.

### 2.2. Target geometry

The target geometry is shown in Fig. 2. The laser light enters through the 300 μm diameter laser entrance hole into the primary hohlraum sphere with a diameter of 600 μm. The primary X-rays heat the secondary hohlraum through a second hole of 300 μm in diameter. The cylindrical secondary hohlraum has a diameter of 1000 μm and a length of 950 μm. The apertures for the ion beam are 800 μm. Extra shielding on the top and back sides is added to keep the ion interaction path free from debris of the rapidly

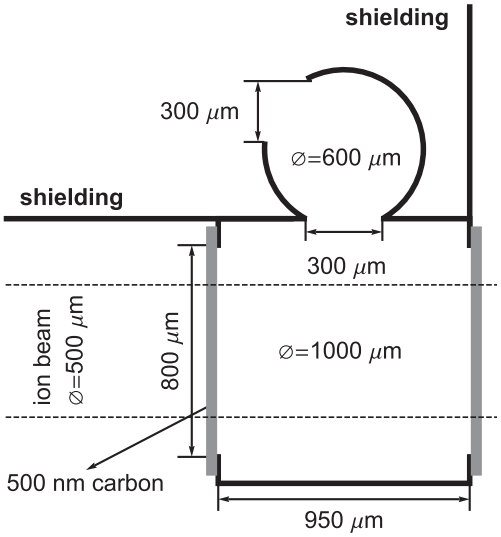


**Fig. 2.** Geometry and dimensions of the double hohlraum target consisting of a primary spherical cavity and a secondary cylindrical hohlraum. Shielding is added on the top and the front to keep debris out of the ion beam path. Two thin carbon foils are attached at each side of the cylinder.

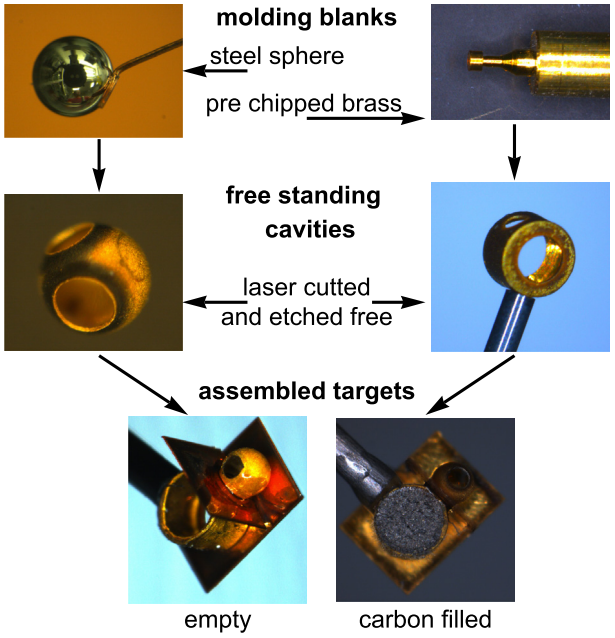


**Fig. 3.** Different steps of target fabrication. The moulding blanks are electroplated with a thin gold layer and then etched out. The holes, the shieldings and the carbon foils are cut out with a laser. All parts are built together under a microscope using micro assembling stages.

expanding primary cavity. Two thin carbon foils, each with an areal density of 100 μg/cm$^2$, are attached on both sides of the cylinder.

### 2.3. Experimental parameters and diagnostics

The primary hohlraum is heated by a 150 J laser pulse of duration 1.2 ns at a 527 nm laser wavelength. The radiation temperatures in the primary and secondary hohlraum are both measured by a streaked X-ray spectrometer through an additional 150 μm diagnostic hole in the hohlraum wall. In the previous experiments, the primary spherical cavity was additionally characterized with an absolutely calibrated diode spectrometer and a time-integrating XUV spectrometer [23]. The electron density of the outflowing carbon plasma is measured time-resolved with a Nomarski multiframe interferometer [29], which is also used as shadowgraphy to characterize the hydrodynamic expansion of the gold.

To confirm that the ablated gold does not influence the ion beam, an empty hohlraum was probed by a calcium ion beam. After a time-of-flight distance of 12 m, the probe beam is stopped in a specially developed polycrystalline CVD diamond detector [30], which allows time resolved measurements of the ion-beam intensity over more than 50 μs. The ion beam first passes through a 500 μm aperture, then through the hohlraum cylinder, and is finally focused onto the stop or charge state detector. The heavy ion beam from the UNILAC accelerator has a bunch frequency of 108 MHz, which results in an ion signal every 9 ns registered by the detector. Each of these ion bunches has a width of 3 ns at FWHM. This pulse length determines the minimum measurement time needed to probe the plasma state. The hohlraum target is designed in such a way that the carbon plasma is maintained for at least 5 ns for the measurements, before it gets disturbed by the gold from the walls. The temporal position of every ion bunch can be determined to an accuracy better than 0.1 ns by fitting the detector signals and determining their centroids.

### 2.4. Target fabrication

The hohlraum targets are manufactured in the Target Laboratory at Technische Universität Darmstadt. First, positive blanks of either brass or steel are formed by micro-chipping and then electroplated with a 15 μm gold layer. Then, the necessary holes are cut into the gold wall with a laser cutter and the blanks are etched out. The shieldings are directly cut out from 25 μm thick gold foils and the sample material from 500 nm thick carbon foils. Finally all parts are assembled with the help of micro positioning stages under a microscope. All components can be fabricated and positioned with an accuracy of ±5 μm. The main fabrication steps and the final targets are shown in Fig. 3.

## 3. Theoretical methods: the RALEF-2D code

Both the primary spherical and the secondary cylindrical hohlraums have been extensively studied by means of 2D hydrodynamic simulations. All the results, presented below, were obtained with the radiation-hydrodynamics code RALEF-2D (Radiative Arbitrary Lagrangian–Eulerian Fluid dynamics in two Dimensions) [31], whose hydrodynamics part is based on an updated version of the CAVEAT hydrodynamics package [32]. The one-fluid one-temperature hydrodynamic equations are solved in two spatial dimensions (in either Cartesian $x,y$ or axisymmetric $r,z$ coordinates) on a multi-block structured quadrilateral grid by a second-order Godunov-type numerical scheme. Mesh rezoning and remapping is performed within the Arbitrary Lagrangiane Eulerian (ALE) approach to numerical hydrodynamics. The code includes thermal conduction and, most importantly, energy transport by thermal radiation in its description of laser-generated plasmas. For this purpose, the 2D hydrodynamics package is coupled with the numerical solution of the equation of spectral radiation transfer in a quasi-static approximation (i.e. with the time derivative of the radiation intensity $I_\nu$ ignored). In each spectral group, the radiation transfer equation is solved by combining the method of short characteristics with the $S_N$ angular quadrature. The simulations discussed below have been performed with $S_N = S_{12}$ and 24 spectral groups. The equation of state, thermal conductivity, and spectral opacities used in these simulations were provided by the THERMOS code [33]. Some additional information on the RALEF-2D code can be found in [31,17].

## 4. Primary hohlraum: X-ray conversion and plasma closure

The optimal configuration of the primary spherical hohlraum is determined by a trade-off between the following requirements. On the one hand, the hohlraum size and the diameter of the entrance hole should be sufficiently large, so that the plasma closure does not cut the laser pulse before its energy is completely deposited inside the hohlraum. On the other hand, they have to be as small as possible to minimize radiation losses and achieve a high temperature inside the hohlraum cavity. To obtain the most efficient conversion from laser light into X-rays, the hohlraum parameters should be carefully adapted to such laser parameters as the wavelength, pulse duration and focus diameter.

Various sphere diameters and hole sizes have been experimentally investigated in the past. The final design, presented in this paper, is based on the best compromise found in the experiments and confirmed by numerical simulations.

In the experiment the radiation emitted through a small diagnostic hole of 150 μm is measured time and spectrally resolved with an XUV grating and X-ray streak camera behind. To determine a corresponding radiation temperature $T_r$, the shapes of the obtained spectra were fitted for each time step with a Planckian curve. These temperature values were then used to get a temporal evolution and the maximum of the radiation temperature inside the primary hohlraum. The results of this measurement are shown in Fig. 4d together with the results from simulations. The measurements reveal a maximum radiation temperature in the primary spherical hohlraum of $(98 \pm 5)$ eV. This value agrees well with common scaling laws for spherical cavities [34,35] which predict $\approx 100$ eV. A detailed discussion of the experimental methods for the radiation temperature measurement was recently published separately by the authors [23,36,24].

In the numerical simulations, the temporal profile of the laser pulse was approximated by a trapezoid, and the transverse spatial profile of the intensity was assumed to be Gaussian (FWHM = 100 μm). The temporal profile of the experimental laser pulse and its approximation for simulations are shown in Fig. 5. In the simulation, the light enters through the 300 μm laser entrance hole, and the emitted X-rays are registered through a 150 μm diagnostic hole by two imaginary spectrometers, positioned at angles 90° and 45° relative to the laser axis — as indicated in Fig. 6. The laser beam is assumed to be parallel without any spatial divergence because of the large focal length of 4 m of the lens used in the experiment, which corresponds to a Rayleigh length of above 1 mm.

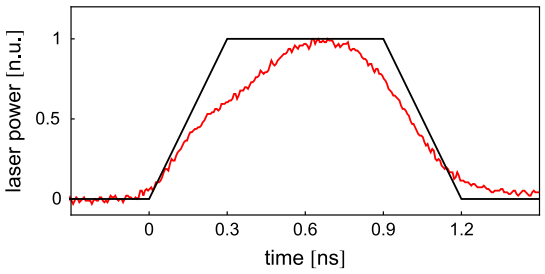


**Fig. 5.** Normalized temporal profile of the laser power used to heat the spherical gold cavity. In the simulations the temporal shape was approximated by a trapezoid.

It should be noted here that a spherical hohlraum with two misaligned holes is essentially a three-dimensional configuration. To simulate it with a 2D code, we had to replace the sphere with a cylinder of the same radius, and perform rescaling of the laser energy in such a way as to preserve as close correspondence with the 3D case as possible. The details of the employed rescaling procedure are described in Ref. [17].

Fig. 4a shows how the laser power $q$ is absorbed inside the primary hohlraum, first at $t = 0.3$ ns by the gold wall and later at $t = 0.9$ ns in the gold plasma which fills up the cavity. The free electron density of the expanding gold plasma along the laser entrance channel varies within the range $n_e = 10^{19} - 10^{21}$ cm$^{-3}$ over the first 1.2 ns. Because the critical density for $\lambda = 527$ nm is $n_c = 4 \times 10^{21}$ cm$^{-3}$, the plasma remains undercritical for the

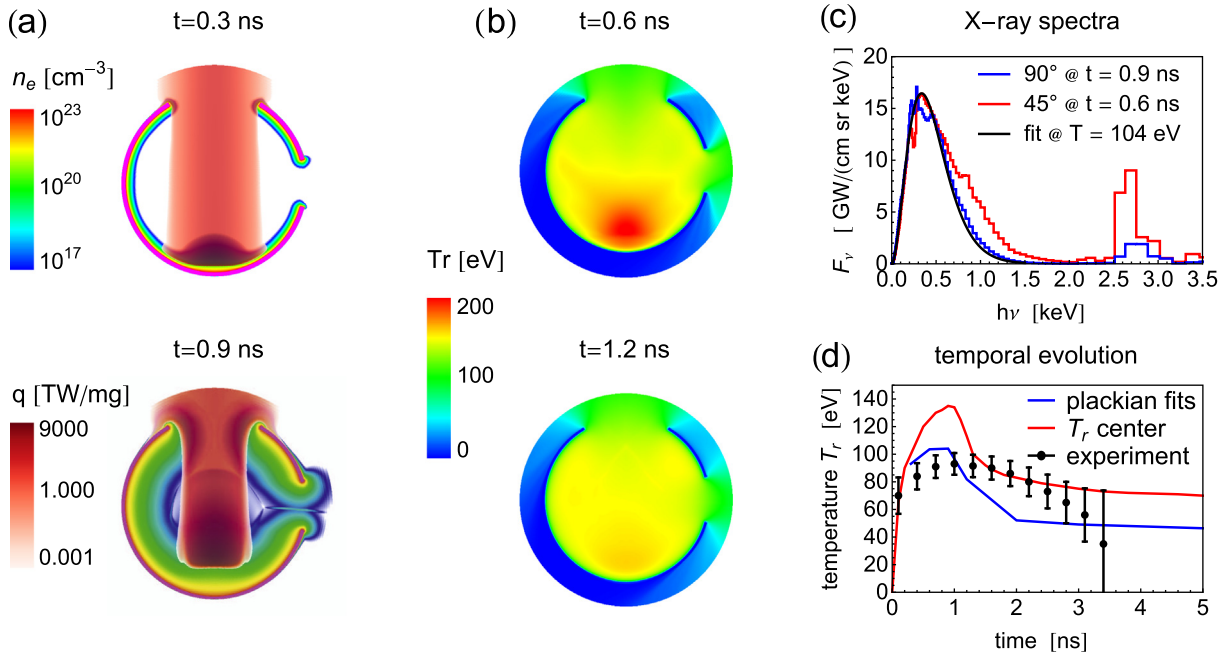


**Fig. 4.** Color contour plots of (a) the deposited laser power $q$ superimposed on the free electron density, (b) the radiation temperature $T_r$ inside the hohlraum. The plasma, filling up the laser entrance hole, stays undercritical over the entire duration of the laser pulse 1.2 ns. (c) Calculated spectra as would have been observed by imaginary spectrometers placed at 90° and 45°. (d) Temporal evolution of the radiation temperature in the center of the hohlraum compared with the Planckian fits to the theoretical and experimental spectra at 90°.

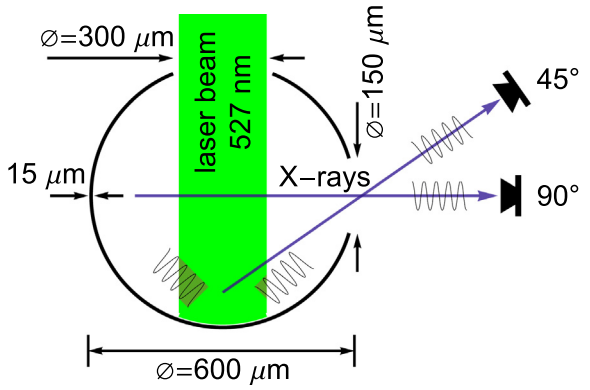


**Fig. 6.** Simulation setup for the primary hohlraum with two holes: one for the laser entrance, and the other for diagnostics. The emitted spectrum is recorded with two imaginary spectrometers at 90° and 45°.

entire pulse duration and the laser deposits its energy deep inside the hohlraum cavity without being reflected.

Fig. 4b shows contour plots of the radiation temperature $T_r$ in the cavity at 0.6 ns, when the laser power reaches its maximum, and at 1.2 ns just after the laser is turned off. As the laser hits the gold wall, a hot spot is created. After a few hundred picoseconds the hohlraum thermalizes and a smooth radiation temperature distribution is reached. The spectral power $F_\nu$ [GW cm$^{-1}$ sr$^{-1}$ keV$^{-1}$], registered by two imaginary detectors at 90° and at 45°, is obtained by integrating the spectral intensity along an imaginary observation slit perpendicular to the corresponding line of sight. Thereby, the 90° detector measures the thermal spectrum emerging from the hohlraum wall section, which is not directly illuminated by the laser. In contrast, the 45° detector looks directly into the hot plasma plume and detects strong line emission from the gold plasma corona in hard X-rays between 2.5 keV and 2.7 keV. The two corresponding lines of sight are indicated with arrows in Fig. 6. Examples of the recorded spectra are shown in Fig. 4c.

It is seen that the emitted spectrum splits up into a thermal part, ranging from 0 keV to 2 keV, and a hard part dominated by line emission (2–4 keV). In terms of total energy this hard part plays a minor role because more than 90% of the emitted radiation power is concentrated in the thermal part. This is easily verified by comparing the integral over frequency, time and solid angle of the thermal part with the same integration over the hard part.

Fig. 4d shows the temporal evolution of the radiation temperature. Shortly after the laser pulse is turned off at 1.2 ns the radiation and matter temperature come close to equilibrium and the hohlraum begins to cool down. However, due to the reheating of the hohlraum center caused by the hydrodynamic flow, the radiation temperature stabilizes between 2 ns and 5 ns at $T_r \approx 80$ eV. Here the theoretical "bolometric" radiation temperature $T_r$ in the hohlraum center is compared to the temperatures obtained from the Planckian fits to the theoretical 90° spectra, and to the experimental results measured at the same angle. The discrepancy between the "bolometric" temperature $T_r$ and the Planckian fits can be explained by the method of calculating $T_r$, which is defined in terms of the full integral,

$$T_r = \left(\frac{1}{4\sigma}\int_0^\infty d\nu \int_{4\pi} I_\nu(\Omega)\, d\Omega\right)^{1/4}, \qquad (2)$$

of the calculated spectral intensity $I_\nu$ over all the frequencies $\nu$ and all the angles $\Omega$; here $\sigma$ is the Stefan–Boltzmann constant. In contrast, the Planckian fits represent the color temperature of the soft thermal part of the emitted X-ray spectrum, and in our case it is these values which allow direct comparison between the experiment and simulations. As can be seen in Fig. 4d, the measured values are in fairly good agreement with those obtained in simulations. Note that here no perfect agreement can be expected simply because the simulated 2D problem is not fully equivalent to the essentially 3D experimental arrangement.

In conclusion, the simulations for the given geometry of the primary hohlraum predict that the plasma closure is sufficiently slow to allow full laser energy deposition inside the cavity. The simulations are validated by precise experimental measurements of the emitted radiation spectra. Further details on these simulations, especially on the numerics and the simulation setup, can be found in [37].

## 5. Secondary hohlraum empty: blowoff of the gold walls

The secondary cylindrical hohlraum is used to generate a plasma column along the propagating ion beam by means of soft X-ray heating. For precise measurements it is crucial that fast ions interact with a pure carbon-plasma channel, which is not contaminated by gold ablated from the hohlraum walls. Hence, the blowoff of the gold walls has to be controlled experimentally and adequately modeled in simulations.

As already mentioned, the ion beam has a diameter of 500 μm, the minimum probing time is about 3 ns, and the time window within which the probing channel should stay free of gold is about 5 ns. To determine the best target geometry, multiple simulations with different cylinder diameters where carried out. The minimum diameter to guarantee this specification was found to be 1000 μm. Experimentally, the influence of the gold plasma on the ion beam was measured by heating up an empty hohlraum with full laser energy and probing it with the ion beam. If the ion beam gets disturbed by the gold plasma from the walls, a clear signature can be seen in the ion beam signal recorded at the stop detector.

The radiation temperature of the secondary hohlraum is again recorded time resolved by an X-ray streak camera behind a spectrometer. The maximum radiation temperature measured in the secondary hohlraum is $(33 \pm 2)$ eV. The measured temporal evolution of the radiation temperature, shown in Fig. 7b, is in good

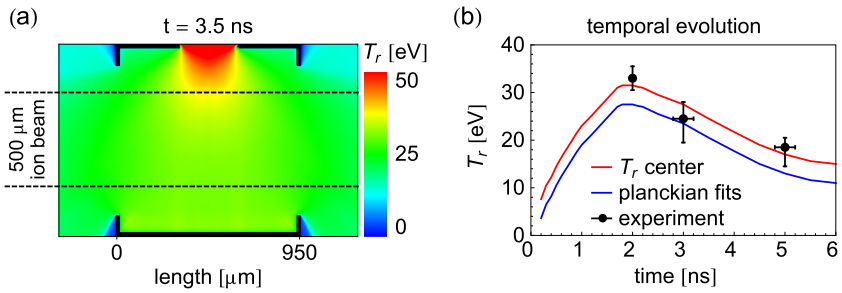


**Fig. 7.** (a) Contour plot of the radiation temperature inside the secondary hohlraum at $t = 3.5$ ns. (b) Temporal evolution of the radiation temperature in the secondary hohlraum.

agreement with the simulated results discussed below. The detailed experimental methods and radiation measurements for various hohlraum geometries are to be published elsewhere [38].

In the simulations, the cylindrical hohlraum is heated by a blackbody spectrum, applied as a boundary condition on the incoming radiation intensity $I_\nu$ along the entrance hole of 300 μm in diameter at the top of the cylinder. The temporal profile of the incoming radiation temperature is directly given by the experimentally measured output profile of the primary hohlraum as shown in Fig. 4d. To characterize the emitted spectra, an imaginary spectrometer with the line of sight along the cylinder axis is used.

As an example, Fig. 7a shows the 2D distribution of the "bolometric" radiation temperature inside the secondary hohlraum at $t = 3.5$ ns. The radiation is distributed quite uniformly, and the sample material, attached to the end of the cylinder, should be heated fairly uniformly as well. In Fig. 7b the simulated radiation temperature in the hohlraum center is compared with the temperature obtained by fitting the simulated spectra. The above discussion about the difference between the two curves applies to the secondary hohlraum as well. The radiation temperature reaches a maximum of $T_r = 32$ eV at $t \approx 2$ ns. After this the hohlraum gradually cools down but stays for about 5 ns above 15 eV. This must ensure a uniform heating of the sample plasma over the entire probing period.

Fig. 8a shows a contour plot of the free electron density at $t = 5$ ns. The solid black contour line indicates the intersection to an electron density below $n_e < 10^{17}$ cm$^{-3}$ (which originates from the initial fill of the presumably empty secondary hohlraum with the low-density gold vapor). The inner wall surface expands with an average velocity of 60 μm/ns towards the cylinder axis. The gold plasma reaches the ion beam channel after 5 ns. This time should be somewhat extended when the carbon plasma is added because the expanding carbon plasma pushes back and slows down the gold expansion.

The plasma closure of the secondary hohlraum is determined by probing an empty hohlraum at a full laser power shot with $^{48}Ca^{17+}$ ions with an energy of 3.5 MeV/u = 168 MeV. For a systematic characterization, the laser ion beam delay is varied between 0 ns and 9 ns. The results of these measurements in terms of a delayed arrival of the ion bunch are shown in Fig. 8b. The shaded area indicates the time window of 5 ns that should stay free of gold for clean energy loss and charge state measurements. Within the accuracy of the detector, no significant disturbance in the time window of interest could be detected. As a consequence, we can assume that the hohlraum center on the ion beam axis stays free of gold as predicted by the simulations.

Time resolved shadowgraphic and interferometric imaging of the plasma flow in the double hohlraum target has shown that the plasma from the primary hohlraum expands very fast. First ablation of gold plasma on the back side of the primary hohlraum wall, where the laser hot spot burn through appears after 3.5 ns. To prevent possible disturbance from debris of the exploding primary hohlraum, which is blown into the ion beam path, additional shielding is attached on the top and the back of the target as indicated in Figs. 2 and 3.

## 6. Secondary hohlraum with carbon fill: evolution and parameters of the sample plasma

To be able to compare the measured ion energy losses with theoretical predictions, it is important to know the plasma parameters along the ion trajectories. Beside the projectile energy and charge state, theoretical models need as an input the density, temperature and ionization degree of the sample plasma [39].

Experimental determination of these quantities in a dense plasma of submillimeter size is a challenging task, and especially so because the plasma properties inside the hohlraum are difficult to access. Common spectroscopic methods to determine the temperature and the ionization degree can not be applied because the line emission of the carbon plasma is completely dominated by the background thermal radiation. Also, plasma interferometry usually used for electron density measurements is limited by the high density and strong gradients. Furthermore, the interferometry as well as shadowgraphy are not able to measure density distributions inside the hohlraum due to the opaqueness of the high-Z wall material. Thus, to get adequate information on the sample carbon plasma, one has to rely on simulations which are benchmarked by experimental measurements.

The simulation setup for the carbon filled secondary hohlraum is the same as for the empty one but with two additional thin carbon foils attached to each end of the cylinder (see Fig. 2a). To speed up the simulation, the carbon foils used in the experiment with an initial density of 1.8 g/cm$^3$ and a thickness of 500 nm were modeled with carbon foils of twice the thickness but half the density, so that the areal density of the real and simulated foil remains the same ($\approx 100$ μg/cm$^2$).

As an illustration, Fig. 9a shows a contour plot of the free electron density at $t = 3.5$ ns. It is seen that the spatial variations in the transverse (with respect to the ion beam) direction are small, so that each projectile ion within the beam aperture sees the same plasma states. The variation of the plasma parameters like temperature, density and ionization across the ion beam profile is less than $< 5\%$. This is of major importance because the energy loss and the charge distribution are measured by detectors which integrate over the whole beam diameter. The advantage of using a hohlraum for creation of quasi-uniform plasma states is stipulated by the fact that the plasma is inertially and thermally confined by the hohlraum walls, which allows to maintain its state for several nanoseconds. This is highlighted in Fig. 9b, where the electron density is plotted as a function of the areal density and time. Most of

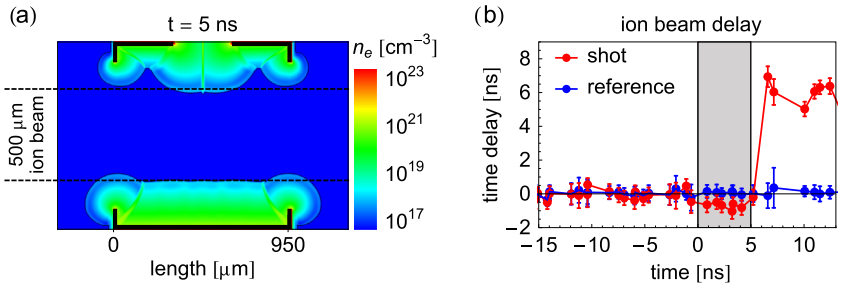


**Fig. 8.** (a) Contour plot of the free electron density of the gold walls inside the secondary hohlraum at $t = 5$ ns. (b) Measured time delay of the ion beam probing the empty hohlraum without laser (blue: reference) and with laser at full energy shot conditions (red: shot). First influence of the gold plasma on the ion beam appears after 5 ns. (For interpretation of the references to color in this figure legend, the reader is referred to the web version of this article.)

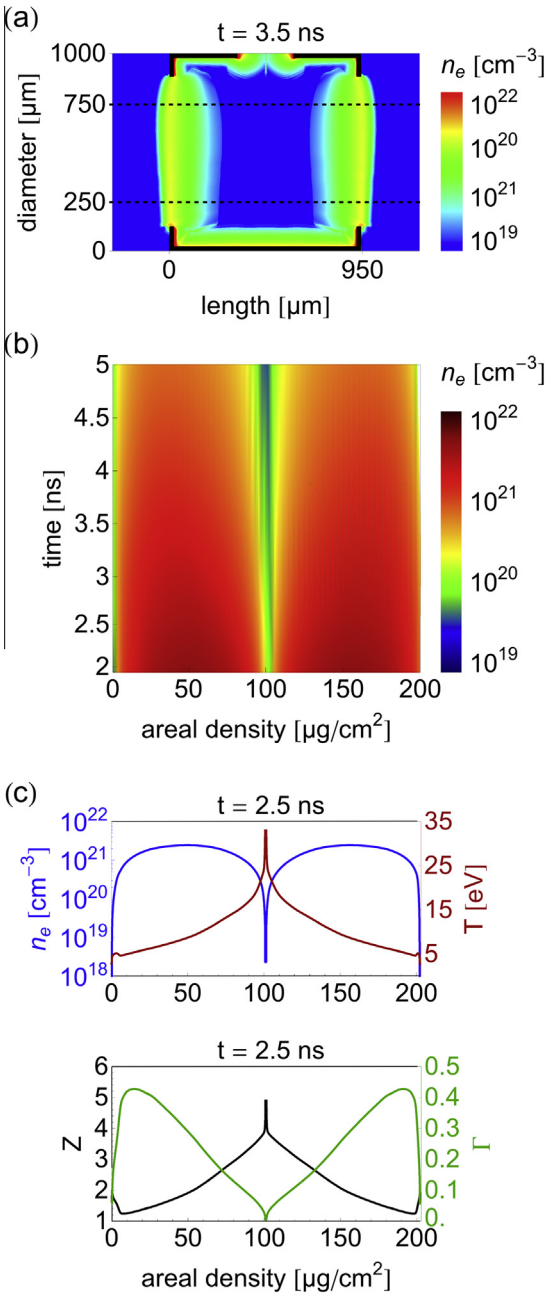


**Fig. 9.** (a) Color contour plot of the free electron density distribution at $t = 3.5$ ns. (b) Evolution of the electron density over time as a function of the areal density. (c) Lineouts of the plasma parameters plotted over the areal density at $t = 2.5$ ns.

the matter ($> 80\%$) stays at high densities above $1 \times 10^{21}$ cm$^{-3}$ for more than 5 ns. Contrary to a directly heated laser plasma, no hot and rapidly expanding corona exists. The sample material is volumetrically heated with strong gradients at the edges. However, a closer inspection of the transversal profile of the plasma parameters, shown in Fig. 9c, reveals that the projectile passes through a variety of plasma states. Especially the temperature and the ionization degree show significant variation between the cold dense outer parts and the dilute but hot plasma in the hohlraum center. The maximum free electron density of $8 \times 10^{21}$ cm$^{-3}$ is achieved at 2 ns. Integrating the electron density over the ion trajectory and taking the time average between 2 ns and 5 ns, we calculate a mean line density of $\int n_e dl \approx 4 \times 10^{20}$ cm$^{-2}$, where the line density varies between $2 \times 10^{20}$ cm$^{-2}$ at $t = 2$ ns to $5 \times 10^{20}$ cm$^{-2}$ at $t = 5$ ns. The plasma coupling parameter is calculated by using Eq. (1). More than 80% of the plasma is in a moderately coupled state with $0.1 < \Gamma < 0.6$.

Experimentally, the carbon plasma flowing out of the secondary hohlraum was investigated with a combined multiframe interferometry, which allowed to record a series of 4 images within 6 ns, each image being separated by 2 ns and time integrated over 0.5 ns. The plasma was probed by a frequency tripled laser at 355 nm, which could theoretically allow measurements of the free electron density up to the critical density of $n_c = 8.8 \times 10^{21}$ cm$^{-3}$. However, due to strong deflection of the probe beam at steep density gradients, almost no fringes could be detected above the electron density of $1 \times 10^{20}$ cm$^{-3}$. The resulting interferograms serve rather as shadowgrams, where the opaque region represents the expanding plasma cloud.

Before $t = 5$ ns no information about the free electron density could be extracted. After that time the gradients of the outer part of the expanding plasma are flattening out and enough fringes appear for a reliable calculation of the free electron density. As an illustration, Fig. 10a shows the experimental results for $t = 5.4$ ns, which are in good agreement with the simulated density profile. The distance indicated is measured from the carbon foil surface.

The displacement of the edge of the shadow over time can be used to determine the expansion velocity of the plasma. Fig. 10b plots the time dependence of this displacement together with the theoretical displacement of the $n_e = 1 \times 10^{20}$ cm$^{-3}$ front, obtained from the RALEF simulation. Both the total displacement in micrometers and the evaluated expansion velocity of $v_{exp} = (70 \pm 15)$ km/s agree fairly well with the corresponding values [$v_{sim} = (60 \pm 2)$ km/s] obtained from the simulation.

On the whole, we observe that the experimental measurements of the outer part of the carbon plasma cloud are in a good accord with the RALEF simulations. This justifies our assumption that the RALEF code should also adequately reproduce the plasma conditions inside the secondary hohlraum, and that the simulated plasma parameters could be used for further theoretical estimates

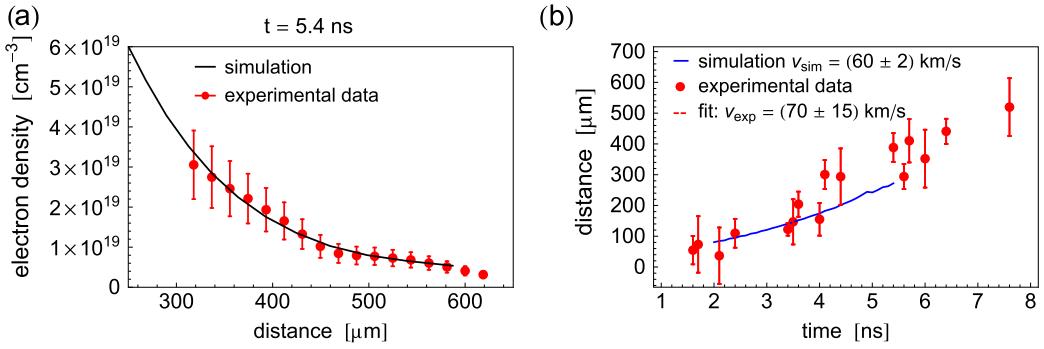


**Fig. 10.** (a) Interferometricaly measured and simulated spatial profiles of the free electron density at $t = 5.4$ ns. The distance is measured from the carbon foil surface. (b) Experimentally measured and simulated expansion velocity of the carbon plasma.

of the energy loss and charge states of fast ions passing through the sample plasma.

## 7. Conclusion

We presented the results on a new double hohlraum target for generation of dense, partly ionized, non-ideal and moderately coupled plasmas ($0.1 < \Gamma < 1$). The hohlraum target and the generated carbon plasma are well described by simulations that have been confirmed by experimental measurements. A quasi-thermal X-ray radiation with an effective temperature of $T_r \approx 30$ eV heats two solid carbon foils to a plasma state with the temperature between $T = 5$ eV and 15 eV, and the free electron density in the range $(1-5) \times 10^{21}$ cm$^{-3}$ — with the peak value reaching $8 \times 10^{21}$ cm$^{-3}$. The partially ionized carbon plasma has an ionization degree of 3.2–3.8. The interaction path of the ion beam stays free of gold for about 5 ns. This has been shown by simulations and confirmed by ion beam measurements.

The generation of a millimeter sized moderately coupled plasma by means of indirect laser heating allows to enter a new regime of interaction of fast heavy ions with plasmas, for which no experimental data exist so far. In particular, these targets are currently used in experiments at GSI, Darmstadt to measure precisely the energy loss and the charge state distribution of heavy ion beams after passing through such a plasma [40].

These targets might further be used for new types of ion stopping experiments, like stopping of slow ions near the maximum of the stopping power [41], or stopping of laser accelerated ions [42]. Another application might be to use them as millimeter sized single-shot plasma lenses.

## Acknowledgments

We wish to acknowledge the expert support of the PHELIX and the UNILAC team at GSI. This work was supported by the Helmholtz International Center for FAIR, by the Extreme Matter Institute EMMI, by the Bundesministerium für Bildung und Forschung BMBF (Project 05P12RFFTR) and by the Jülich Supercomputing Centre JSC.

## References

[1] D.D.M. Ho, J.A. Harte, M. Tabak, Configurations of radiation driven targets for heavy ion fusion, Nucl. Fusion 35 (9) (1995) 1125–1132, http://dx.doi.org/10.1088/0029-5515/35/9/I06.
[2] B.G. Logan, L.J. Perkins, J.J. Barnard, Direct drive heavy-ion-beam inertial fusion at high coupling efficiency, Phys. Plasmas 15 (7) (2008) 072701, http://dx.doi.org/10.1063/1.2950303.
[3] M. Roth, T. Cowan, M. Key, S. Hatchett, C. Brown, W. Fountain, J. Johnson, D. Pennington, R. Snavely, S. Wilks, K. Yasuike, H. RUHL, F. Pegoraro, S. Bulanov, E. Campbell, M. Perry, H. Powell, Fast ignition by intense laser-accelerated proton beams, Phys. Rev Lett. 86 (3) (2001) 436–439, http://dx.doi.org/10.1103/PhysRevLett. 86.436.
[4] D.H.H. Hoffmann, K. Weyrich, H. Wahl, D. Gardés, R. Bimbot, C. Fleurier, Energy loss of heavy ions in a plasma target, Phys. Rev. A 42 (1990) 2313–2321, http://dx.doi.org/10.1103/PhysRevA.42.2313.
[5] D. Gardes, A. Servajean, B. Kubica, C. Fleurier, D. Hong, C. Deutsch, G. Maynard, Stopping of multicharged ions in dense and fully ionized hydrogen, Phys. Rev. A 46 (1992) 5101–5111, http://dx.doi.org/10.1103/PhysRevA.46.5101.
[6] K.-G. Dietrich, D.H.H. Hoffmann, E. Boggasch, J. Jacoby, H. Wahl, M. Elfers, C.R. Haas, V.P. Dubenkov, A.A. Golubev, Charge state of fast heavy ions in a hydrogen plasma, Phys. Rev. Lett. 69 (1992) 3623–3626, http://dx.doi.org/10.1103/PhysRevLett. 69.3623.
[7] J. Jacoby, D.H.H. Hoffmann, W. Laux, R.W. Müller, H. Wahl, K. Weyrich, E. Boggasch, B. Heimrich, C. Stöckl, H. Wetzler, S. Miyamoto, Stopping of heavy ions in a hydrogen plasma, Phys. Rev. Lett. 74 (1995) 1550–1553, http://dx.doi.org/10.1103/PhysRevLett. 74.1550.
[8] C. Couillaud, R. Deicas, P. Nardin, M.A. Beuve, J.M. Guihaumé, M. Renaud, M. Cukier, C. Deutsch, G. Maynard, Ionization and stopping of heavy ions in dense laser-ablated plasmas, Phys. Rev. E 49 (1994) 1545–1562, http://dx.doi.org/10.1103/PhysRevE.49.1545.
[9] M. Roth, C. Stökel, W. Sü, O. Iwase, D. Gericke, R. Bock, D. Hoffmann, M. Geissel, W. Seelig, Energy loss of heavy ions in laser-produced plasmas, Europhys. Lett. 50 (2000) 28–34, http://dx.doi.org/10.1209/epl/i2000-00230-6.
[10] A. Frank, A. Blažežević, P.L. Grande, K. Harres, T. Heßling, D.H.H. Hoffmann, R. Knobloch-Maas, P.G. Kuznetsov, F. Nürnberg, A. Pelka, G. Schaumann, G. Schiwietz, A. Schökel, M. Schollmeier, D. Schumacher, J. Schütrumpf, V.V. Vatulin, O.A. Vinokurov, M. Roth, Energy loss of argon in a laser-generated carbon plasma, Phys. Rev. E 81 (2010) 026401, http://dx.doi.org/10.1103/PhysRevE.81.026401.
[11] A. Tauschwitz, M. Basko, A. Frank, V. Novikov, A. Grushin, A. Blažević, M. Roth, J. Maruhn, 2D radiation-hydrodynamics modeling of laser-plasma targets for ion stopping measurements, HEDP 9 (2013) 158–166, http://dx.doi.org/10.1016/j.hedp.2012.12.004.
[12] A. Frank, A. Blažežević, et al., Energy loss and charge transfer of argon in a laser-generated carbon plasma, Phys. Rev. Lett. 110 (2013) 115001, http://dx.doi.org/10.1103/PhysRevLett. 110.115001.
[13] J. Hasegawa, H. Ikagawa, S. Nishinomiya, T. Watahiki, Y. Oguri, Beam–plasma interaction experiments using electromagnetically driven shock waves, Nucl. Instr. Meth. A 606 (1–2) (2009) 205–211, http://dx.doi.org/10.1016/j.nima.2009.03.102.
[14] K. Katagiri, J. Hasegawa, S. Nishinomiya, H. Ikagawa, Y. Oguri, Time-resolved measurement of a shock-driven plasma target for interaction experiments between heavy ions and plasmas, J. Appl. Phys. 102 (11) (2007) 113304.
[15] K. Weyrich, H. Wahl, D. Hoffmann, A.A. Golubev, A.V. Kantsyrev, B.Y. Sharkov, M. Kulish, S. Dudin, V.B. Mintsev, V.E. Fortov, V. Gryaznov, Shockwave-driven, non-ideal plasmas for interaction experiments with heavy-ion beams, J. Phys. A: Math. Gen. 39 (17) (2006) 4749–4754, http://dx.doi.org/10.1088/0305-4470/39/17/S69.
[16] O.N. Rosmej, V. Bagnoud, U. Eisenbarth, V. Vatulin, N. Zhidkov, N. Suslov, A. Kunin, A. Pinegin, D. Schäfer, T. Nisius, T. Wilhein, T. Rienecker, J. Wiechula, J. Jacoby, Y. Zhao, G. Vergunova, N. Borisenko, N. Orlov, Heating of low-density CHO-foam layers by means of soft X-rays, Nucl. Instr. Meth. A 653 (1) (2011) 52–57, http://dx.doi.org/10.1103/PhysRevA.72.052901.
[17] S. Faik, A. Tauschwitz, M.M. Basko, J. Maruhn, O. Rosmej, T. Rienecker, V. Novikov, A.S. Grushin, Creation of a homogeneous plasma column by means of hohlraum radiation for ion-stopping measurements, HEDP 10 (2014) 47–55, http://dx.doi.org/10.1016/j.hedp.2013.10.002.
[18] K. Eidmann, T. Kishimoto, Absolutely measured X-ray spectra from laser plasmas with targets of different elements, Appl. Phys. Lett. 49 (7) (1986) 377, http://dx.doi.org/10.1063/1.97592.
[19] I.B. Földes, R. Pakula, S. Sakabe, R. Sigel, Light absorption in laser-heated cavities, Appl. Phys. B 43 (2) (1987) 117–122, http://dx.doi.org/10.1007/BF00692826.
[20] R. Sigel, The generation of intense Planck radiation by laser, Plasma Phys. Controlled Fusion 29 (10A) (1987) 1261–1272.
[21] H. Nishimura, Y. Kato, H. Takabe, T. Endo, K. Kondo, H. Shiraga, S. Sakabe, T. Jitsuno, M. Takagi, C. Yamanaka, S. Nakai, R. Sigel, G. Tsakiris, J. Massen, M. Murakami, F. Lavarenne, R. Fedosejevs, J. Meyer-ter Vehn, K. Eidmann, S. Witkowski, X-ray confinement in a gold cavity heated by 351-nm laser light, Phys. Rev. A 44 (12) (1991) 8323–8333, http://dx.doi.org/10.1103/PhysRevA.44.8323.
[22] J. Lindl, Development of the indirectdrive approach to inertial confinement fusion and the target physics basis for ignition and gain, Phys. Plasmas 2 (1995) 3933, http://dx.doi.org/10.1063/1.871025.
[23] T. Heßling, A. Blaevi, et al., Time- and spectrally resolved measurements of laser-driven hohlraum radiation, Phys. Rev. E 84 (2011) 016412, http://dx.doi.org/10.1103/PhysRevE.84.016412.
[24] D. Schumacher, Investigation of laser driven hohlraum radiation and energy loss of heavy ions in indirectly heated Plasma (Ph.D. thesis), TU Darmstadt, Darmstadt, 2012.
[25] G. Zwicknagel, P.G. Reinhard, C. Seele, C. Toepffer, Energy loss of heavy ions in strongly coupled plasmas, Fusion Eng. Design 32–33 (1996) 523–528, http://dx.doi.org/10.1016/S0920-3796(96)00509-1.
[26] D. Gericke, M. Schlanges, Beam-plasma coupling effects on the stopping power of dense plasmas, Phys. Rev. E 60 (1) (1999) 904–910, http://dx.doi.org/10.1103/PhysRevE.60.904.
[27] D. Gericke, M. Schlanges, T. Bornath, Stopping power of nonideal, partially ionized plasmas, Phys. Rev. E 65 (3) (2002) 036406, http://dx.doi.org/10.1103/PhysRevE.65.036406.
[28] V. Bagnoud, B. Aurand, A. Blažević, S. Borneis, C. Bruske, B. Ecker, U. Eisenbarth, J. Fils, A. Frank, E. Gaul, S. Goette, C. Haefner, T. Hahn, K. Harres, H.-M. Heuck, D. Hochhaus, D. Hoffmann, D. Javorkov, H.-J. Kluge, T. Kuehl, S. Kunzer, M. Kreutz, T. Merz-Mantwill, P. Neumayer, E. Onkels, D. Reemts, O. Rosmej, M. Roth, T. Stoehlker, A. Tauschwitz, B. Zielbauer, D. Zimmer, K. Witte, Commissioning and early experiments of the phelix facility, Appl. Phys. B 100 (1) (2010), http://dx.doi.org/10.1007/s00340-009-3855-7.
[29] M. Börner, J. Fils, A. Frank, A. Blažević, Development of a Nomarski-type multi-frame interferometer as a time and space resolving diagnostics for the free electron density of laser-generated plasma, Rev. Sci. Instrum. 83 (2012) 043501, http://dx.doi.org/10.1063/1.3701366.
[30] W. Cayzac, A. Frank, D. Schumacher, M. Roth, A. Blažević, F. Wamers, M. Träger, E. Berdermann, B. Voss, T. Heßling, A spectrometer on chemical vapour deposition-diamond basis for the measurement of the charge-state distribution of heavy ions in a laser-generated plasma, Rev. Sci. Instrum. 84 (4) (2013) 043301, http://dx.doi.org/10.1063/1.4798539.

[31] M.M. Basko, J. Maruhn, A. Tauschwitz, Development of a 2D radiation-hydrodynamics code RALEF for laser plasma simulations, GSI Scientific Report (GSI Report 2010-1) (2010) 410.
[32] F.L. Addessio, J.R. Baumgardner, J.K. Dukowicz, N.L. Johnson, B.A. Kashiwa, R.M. Rauenzahn, C. Zemach, CAVEAT: A Computer Code for Fluid Dynamics Problems With Large Distortion and Internal Slip, Report LA-10613-MS-Rev. 1, UC-32, Los Alamos National Laboratory (1992).
[33] A. Iacob, A.F. Nikiforov, V.G. Novikov, V.B. Uvarov, Quantum-Statistical Models of Hot Dense Matter, Methods for Computation Opacity and Equation of State, Springer, 2006.
[34] G.D. Tsakiris, Energy redistribution in cavities by thermal radiation, Phys. Fluids B 4 (4) (1992) 992–1005, http://dx.doi.org/10.1063/1.860115.
[35] J. Shao-en, S. Ke-Xu, D. Yong-Kun, H. Tian-Xuan, C. Yan-Li, C. Jui-Sen, Radiation temperature scaling law for gold hohlraum heated with lasers at 0.3 mm wavelength, Chin. Phys. Lett. 22 (9) (2005) 23282331.
[36] D. Schumacher, A. Blažević, A. Frank, T. Heßling, G. Schaumann, M. Roth, First hohlraum shots with the frequency doubled PHELIX laser beam , Tech. Rep. GSI Report 2011-1 (May 2011).
[37] M.M. Basko, J. Maruhn, A. Tauschwitz, V.G. Novikov, A.S. Grushin, On the hohlraum targets for ion stopping measurements in dense hot plasma, GSI Scientific Report (GSI Report 2011–03) (2011) 1–17.
[38] D. Schumacher, A. Ortner, A. Blažević, A. Frank, M. Roth, Temperature measurement of hohlraums for energy loss experiments in indirectly heated carbon plasma, Phys. Rev. E (accepted for publication).
[39] A. Ortner, A. Frank, A. Blažević, M. Roth, The role of charge-transfer in heavy ion beam plasma interaction at intermediate ion energies, Phys. Rev. E (accepted for publication).
[40] A. Ortner, D. Schumacher, et al., A novel experimental setup for energy loss and charge state measurements in dense weakly coupled plasma using laser-heated hohlraum targets, J. Phys: Conf. Ser. (submitted for publication).
[41] W. Cayzac, A. Ortner, A. Frank, et al., Ion energy loss at the stopping-power maximum in a laser-generated plasma, J. Phys: Conf. Ser. (submitted for publication).
[42] M. Gauthier, S.N. Chen, A. Levy, P. Audebert, C. Blancard, T. Ceccotti, M. Cerchez, D. Doria, V. Floquet, E. Lamour, C. Peth, L. Romagnani, J.P. Rozet, M. Scheinder, R. Shepherd, T. Toncian, D. Vernhet, O. Willi, M. Borghesi, G. Faussurier, J. FUCHS, Charge equilibrium of a laser-generated carbon-ion beam in warm dense matter, Phys. Rev. Lett. 110 (13) (2013) 135003, http://dx.doi.org/10.1103/PhysRevLett. 110.135003.